

# A STATISTICAL STUDY OF SUPER-LUMINOUS SUPERNOVAE IN THE MAGNETAR ENGINE MODEL AND IMPLICATIONS FOR THEIR CONNECTION WITH GAMMA-RAY BURSTS AND HYPERNOVAE

YUN-WEI YU<sup>1,2</sup>, JIN-PING ZHU<sup>1</sup>, SHAO-ZE LI<sup>1</sup>, HOU-JUN LÜ<sup>3,4</sup>, YUAN-CHUAN ZOU<sup>5</sup>

*Draft version July 7, 2021*

## ABSTRACT

By fitting the bolometric light curves of 31 super-luminous supernovae (SLSNe) with the magnetar engine model, we derive the ejecta masses and magnetar parameters for these SLSNe. The lower boundary of magnetic field strengths of SLSN magnetars can be set just around the critical field strength  $B_c$  of electron Landau quantization. In more details, SLSN magnetars can further be divided into two subclasses of magnetic fields of  $\sim (1 - 5)B_c$  and  $\sim (5 - 10)B_c$ , respectively. It is revealed that these two subclasses of magnetars are just associated with the slow-evolving and fast-evolving bolometric light curves of SLSNe. In comparison, the magnetars harbored in gamma-ray bursts (GRBs) and associated hypernovae are usually inferred to have much higher magnetic fields with a lower boundary about  $\sim 10B_c$ . This robustly suggests that it is the magnetic fields that play the crucial role in distinguishing SLSNe from GRBs/hypernovae. The rotational energy of SLSN magnetars are found to be correlated with the masses of supernova ejecta, which provides a clue to explore the nature of their progenitors. Moreover, the distribution of ejecta masses of SLSNe is basically intermediate between those of normal core-collapse supernovae and hypernovae. This could indicate an intrinsic connection among these different stellar explosions.

*Subject headings:* gamma-ray burst: general — stars: neutron — supernovae: general

## 1. INTRODUCTION

Superluminous supernovae (SLSNe) are an unusual type of supernovae intrinsically bright with a peak absolute magnitude of  $M < -21$ , which are about 10 – 100 times brighter than normal supernova events (Gal-Yam et al. 2012). The event rate of SLSNe was estimated to several tens to a hundred times per year per cubic gigaparsecs at redshift  $z \sim 1$ , which increases with redshift in a manner consistent with that of the cosmic star formation history (Prajs et al. 2017). As usual, SLSNe can be divided observationally into two classes according to the detection of hydrogen in their spectra, i.e., hydrogen-poor SLSNe I (Quimby et al. 2011) and hydrogen-rich SLSNe II (Ofek et al. 2007; Smith et al. 2007). SLSNe I commonly have a blue continua at peak and a distinctive W-shaped feature identified as O II at early epochs. A few tens of days after peak, their spectral evolution becomes very similar to normal or broad-lined Type Ic supernovae (Pastorello et al. 2010). SLSNe II have a blue continua too at maximum light and, more importantly, some clear Balmer features exist in their spectra. The current observed number of SLSNe I is apparently larger than that of SLSNe II. In addition, for some particular SLSNe (e.g. iPTF13ehe), their spectral type could even evolve from one to another as the fading of the emission (Yan et al. 2015). With one exception (PTF 10uhf), the

host galaxies of SLSNe I are always found to be low-mass and low-metallicity ( $\lesssim 0.5Z_\odot$ ), whereas those of SLSNe II are usually all over the entire range of galaxy masses and metallicities (Neill et al. 2011; Lunnan et al. 2014; Leloudas et al. 2015; Chen et al. 2016a; Angus et al. 2016; Perley et al. 2016).

The energy sources powering SLSNe are puzzling, while the traditional scenario of radioactive decays of heavy elements is seriously challenged by the unusually high luminosity. The total radiated energy of a typical SLSN is about a few times  $10^{51}$  erg. If this radiation is mainly powered as usual by the radioactive chain  $^{56}\text{Ni} \rightarrow ^{56}\text{Co} \rightarrow ^{56}\text{Fe}$ , then an extremely large amount (several to several tens of solar masses) of radioactive nickel is required to be produced during the supernova explosion, which is unfortunately impossible for normal supernova nucleosynthesis (e.g. Umeda & Nomoto 2008). Nevertheless, such a high mass of nickel could still be produced during some unusual supernova explosions that are triggered due to electron-positron pair-production instability (Barkat et al. 1967; Heger & Woosley 2002). Gal-Yam et al. (2009) firstly used this pair-instability supernova (PISN) model to explain the light curve of hydrogen-poor SN 2007bi, which decays very slowly at late phase being consistent with the decay of radioactive nickel and cobalt (cf. see Kozyreva & Blinnikov 2015). In contrast, a counterview was argued by Nicholl et al. (2013) as that the PISN model could be disfavored by the fast rising of two SN 2007bi-like SLSNe. In any case, it is expected that PISNe tend to appear at relatively high redshifts (McCrum et al. 2014), which can significantly suppress their detection probability at relatively near distances. Therefore, even if a few SLSNe can indeed be ascribed to PISNe, most other SLSNe (in particular, the fast evolving ones) inevitably need some other powerful energy sources alternative to radioactivities.

<sup>1</sup> Institute of Astrophysics, Central China Normal University, Wuhan 430079, China, yuyw@mail.ccnu.edu.cn

<sup>2</sup> Key Laboratory of Quark and Lepton Physics (Central China Normal University), Ministry of Education, Wuhan 430079, China

<sup>3</sup> GXU-NAOC Center for Astrophysics and Space Sciences, Department of Physics, Guangxi University, Nanning 530004, China

<sup>4</sup> Guangxi Key Laboratory for Relativistic Astrophysics, Nanning, Guangxi 530004, China

<sup>5</sup> School of Physics, Huazhong University of Science and Technology, Wuhan, China

On one hand, the broad-lined features in SLSN spectra indicate that the supernova ejecta moves at a very high speed and thus carries huge kinetic energy. Therefore, it is natural to consider that the ejecta can be heated by consuming the kinetic energy through shock interaction with circum-stellar material (CSM; Smith & McCray 2007; Moriya et al. 2011, 2013; Chevalier & Irwin 2011; Ginzburg & Balberg 2012), if the CSM is dense and extended sufficiently. It is interesting to mention that such opaque CSM could sometimes be produced by violent pulsation of a massive star triggered by pair instability, before the final disruption of the star (i.e., the pulsational PISN model; Woosley et al. 2007; Chatzopoulos & Wheeler 2012). Observationally, the CSM-interaction model can be strongly supported by the existence of intermediate and narrow Balmer emission lines in the spectra of some SLSNe II termed SLSN IIn. These lines are formed due to recombination of ionized CSM.

On the other hand, usually for hydrogen-poor SLSNe I, it is considered that their emission could be associated with a long-lived central engine, which can release energy persistently. In this case, the supernova ejecta can be heated gradually by absorbing the engine-released energy. Very recently, Inserra et al. (2016a) discovered an axi-symmetric ellipsoidal configuration for the ejecta of SN 2015bn. Such a geometry, which is similar to those of hypernovae associated with gamma-ray bursts (GRBs), strongly indicates the significant influence of a central engine. To be specific, the energy release from a central engine could be due to spin-down of a millisecond magnetar (Ostriker & Gunn 1971; Woosley et al. 2010; Kasen et al. 2010, 2016; Moriya et al. 2016; Chen et al. 2016b) or/and due to fallback accretion (Dexter & Kasen 2013). In comparison, the former scenario was much more adopted in literature, probably because the allowable ranges of luminosities and timescales of magnetar spin-down are much wider than those of fallback accretion (e.g. Yu & Li 2016).

In view of its obvious advantages, the magnetar engine model has been widely employed to explain SLSN emission either individually (e.g., Dessart et al. 2012; Nicholl et al. 2013; Howell et al. 2013; McCrum et al. 2014; Dai et al. 2016) or in bulk (e.g., Inserra et al. 2013, 2016b; Chatzopoulos et al. 2013; Wang et al. 2015; Nicholl et al. 2015a). These works can usually go to success and account for observations usually better than the models of CSM interaction and of radioactive decays. In this paper we try to carry out such a work with the maximum sample possible, in order to reveal some statistical properties of magnetar-powered SLSNe and the corresponding magnetars, and compare the results with statistics of long GRBs and their associated hypernovae. The paper is organized as follows. In Section 2 the magnetar engine model is introduced briefly. In Section 3 we collect observational data of SLSNe from literature and fit the bolometric light curves of the SLSNe with the magnetar model. The statistics of the obtained model parameters are given in Section 4. In Section 5, we discuss the possible connections and differences between SLSNe and GRBs/hypernovae as well as normal Type Ic broad-lined (Ic-BL) supernovae. Summary and conclusion are given in Section 6.

## 2. MAGNETAR ENGINE MODEL

Similar to previous statistical works of SLSNe (e.g., Nicholl et al. 2015a), a simple semi-analytical model is adopted in this paper to calculate the emission of magnetar-powered SLSNe. Following Kasen & Bildsten (2010), the bolometric luminosity of a supernova can be roughly determined by the following formula:

$$L_{\text{sn}} = \frac{cE_{\text{int}}}{R\tau} (1 - e^{-\tau}), \quad (1)$$

which is derived according to the heat diffusion in the supernova ejecta, where  $c$  is the speed of light,  $E_{\text{int}}$  is the total internal energy of the ejecta,  $R$  is the ejecta radius, and  $\tau$  is the optical depth. For an ejecta mass of  $M_{\text{ej}}$ , we can estimate  $\tau = 3\kappa M_{\text{ej}}/4\pi R^2$ , where  $\kappa$  is the opacity. For  $\tau \gg 1$  the above equation reads  $L_{\text{sn}} = cE_{\text{int}}/(R\tau)$ , while  $L_{\text{sn}} = cE_{\text{int}}/R$  for  $\tau \ll 1$  (e.g., see Kotera et al. 2013). For simplicity, a constant value of  $\kappa = 0.1\text{cm}^2\text{g}^{-1}$  is adopted in following calculations, which is typical and reasonable for SLSNe (Inserra et al. 2013; Nicholl et al. 2015a). By considering of the energy conservation of the ejecta, the evolution of its internal energy can be calculated by

$$\frac{dE_{\text{int}}}{dt} = L_{\text{sd}} - L_{\text{sn}} - 4\pi R^2 p v, \quad (2)$$

where  $t$  is the time,  $L_{\text{sd}}$  is the energy injection rate due to spin-down of a magnetar,  $p$  is the pressure that can be related to the internal energy by  $p = \frac{1}{3}(E_{\text{int}}/\frac{4}{3}\pi R^3)$ , and  $v = dR/dt$  is the expansion speed of the ejecta. The term  $4\pi R^2 p v dt$  represents the adiabatic cooling of the ejecta, which energy is used to accelerate the ejecta. Therefore, the dynamical equation can be written as

$$\frac{dv}{dt} = \frac{4\pi R^2 p}{M_{\text{ej}}}. \quad (3)$$

For a dipolar magnetic field of polar strength of  $B_p$ , the spin-down luminosity of a magnetar as a function of time can be expressed by the magnetic dipole radiation formula:

$$L_{\text{sd}} = L_{\text{sd},i} \left(1 + \frac{t}{t_{\text{sd}}}\right)^{-2} \quad (4)$$

with an initial value of  $L_{\text{sd},i} = 10^{47} B_{p,14}^2 P_{i,-3}^{-4} \text{erg s}^{-1}$  and a spin-down timescale of  $t_{\text{sd}} = 2 \times 10^5 B_{p,14}^{-2} P_{i,-3}^2 \text{s}$ , where  $P_i$  is the initial spin period of the magnetar. Hereafter the conventional notation  $Q_x = Q/10^x$  is adopted in cgs units.

The above equations can be solved numerically by taking an initial kinetic energy for the ejecta and assigning values for the model parameters:  $L_{\text{sd},i}$ ,  $t_{\text{sd}}$ , and  $M_{\text{ej}}$ . As a result, the bolometric luminosity of a supernova can be obtained as a function of time<sup>6</sup>. Statistics of normal

<sup>6</sup> The solution is usually approximated by the following integral (Arnett 1982):

$$L_{\text{sn}}(t) = e^{-\left(\frac{t}{t_d}\right)^2} \int_0^t 2L_{\text{sd}}(t') \frac{t'}{t_d} e^{\left(\frac{t'}{t_d}\right)^2} \frac{dt'}{t_d}, \quad (5)$$

where the dynamical evolution of the supernova ejecta is ignored and its heat diffusion timescale is given by  $t_d = (3\kappa M_{\text{ej}}/4\pi v_f c)$ . The final speed of ejecta  $v_f$  can be determined from  $\frac{1}{2}M_{\text{ej}}v_f^2 = (E_{\text{kin},i} + L_{\text{sd},i}t_{\text{sd}} - E_{\text{rad}})$ , where  $E_{\text{rad}}$  is the energy release via ra-

core-collapse supernovae showed that their kinetic energies are concentrated within the range from  $10^{51}$  erg to several times  $10^{51}$  erg (Lyman et al. 2014). It is considered here that the initial trigger processes of SLSN explosions could be similar to those of normal core-collapse supernovae. In this case, the SLSN ejecta could obtain a similar initial kinetic energy on the order of  $10^{51}$  erg, which is taken in our calculations. It should be emphasized that the kinetic energies of most SLSN ejecta can quickly become much larger than this initial value because of the energy injection from magnetar. Therefore, to a certain extent, fittings to observational light curves would not be very sensitive to the choice of the initial value of kinetic energy.

### 3. DATA COLLECTION AND FITTINGS

Up to December 2016, dozens of SLSNe have been discovered by different authors with different telescopes. The consistency of these SLSNe with the magnetar engine model had been individually inspected in literature by modeling their light curves as well as their temperature and velocity evolutions. On one hand, the magnetar model is most favored by SLSNe I. Therefore, we have primarily collected 27 SLSNe I whose bolometric light curves had been given in the literature. Here, two unique transients (i.e. PS1-10afx and ASASSN-15lh), which were classified to SLSNe I initially (Chornock et al. 2013; Dong et al. 2016), are not included in our sample, because the former is likely to be a lensed Type Ia supernova (Quimby et al. 2014) and the latter has very unusual behaviors (Godoy-Rivera et al. 2017) and is even suggested to be a tidal disruption event from a Kerr black hole (Leloudas et al. 2016). On the other hand, for SLSNe II, part of them (i.e., SLSNe II such as CSS100217, SN 2006tf, SN 2006gy, and SN 2008am) can be undoubtedly ascribed to an ejecta-CSM interaction. However, as pointed out by Inserra et al. (2016b), some other SLSNe II, which have only broad  $H\alpha$  features in their early spectra, could still well be explained by the magnetar engine model. Therefore, such four broad-lined SLSNe II (i.e., CSS121015, PS15br, SN 2008es, SN 2013hx) will also be taken into account in our statistics, in order to maximize the sample number.

The basic information of the 31 selected SLSNe is listed in Table 1 including supernova names, spectral types, coordinates, redshifts, and references. From the listed references, we take the light curves of these SLSNe and present them in Figure 1. These light curves are regarded as bolometric as reported in the references and no further correction is made for them in this paper. Technically, for a statistical study, the parameter values of these SLSNe in the magnetar engine model can also be taken directly from the references. Nevertheless, here we choose to refit the bolometric light curves of all 31 SLSNe in a united method as described in Section 2, just for a general self-consistency. The obtained values of model parameters (i.e.,  $L_{sd,i}$ ,  $t_{sd}$ , and  $M_{ej}$ ) are listed in Table 2, which are generally consistent with the results presented in previous literature (e.g. Chatzopoulos et al. 2013). The fitting results are presented in Figure 1. As shown, the light curves can well be fitted by the magnetar engine model during early times, including the rising diation.

and decreasing phases generally until  $\sim 100 - 200$  days after peak.

In despite of the good modelings of the light curve peaks, at late time the fitting curves could sometimes deviate from the observational data. Firstly, for some SLSNe (e.g., LSQ 12dlf, LSQ 14bdq, and PTF 12dam), the theoretical light curves could become higher and higher than the late data, which is probably due to our neglecting of the suppression of energy absorption efficiency<sup>7</sup>. Secondly, as Wang et al. (2016) suggested, while the peak emission is dominated by the engine contribution, the late emission of some SLSNe could be partially contributed by shock interactions and radioactivities. Finally, of more interests, some frequent undulations could appear in the light curves of some SLSNe (e.g., PS1-11ap, PTF10hgi, and SN2015bn), while the underlying profile of these light curves can be explained successfully with a continuous energy injection from a magnetar. These undulations could be caused by collisions of supernova ejecta with some clumping CSM (Nicholl et al. 2016) or by some late intermittent flare activities of the magnetar engine (Yu & Li 2016). In any case, the primary purpose of this paper is just to get a universal set of model parameters for a large enough SLSN sample, which can basically be determined by fitting the light curves around peak. Therefore, detailed emission characteristics of specific SLSNe such as those mentioned above are ignored in our fittings.

### 4. STATISTICS OF MODEL PARAMETERS

#### 4.1. Magnetar parameters

In Figure 2, the spin-down timescales of the SLSN magnetars are displayed against the initial values of spin-down luminosity, where an anti-correlation seems to appear between these two quantities. In fact, such an anti-correlation had also been previously claimed for GRB magnetars, which exhibits as a relationship between the luminosity and duration of the X-ray afterglow plateaus of GRBs (Dainotti et al. 2008; Rowlinson et al. 2014). It is not difficult to understand this relationship by combining the expressions of  $L_{sd,i}$  and  $t_{sd}$ . Specifically, for a fixed magnetic field we have  $L_{sd,i,47} = 5.0B_{p,14}^{-2}t_{sd,day}^{-2}$  or for a fixed initial spin period  $L_{sd,i,47} = 2.3P_{i,-3}^{-2}t_{sd,day}^{-1}$ . These expressions are presented in Figure 2 by the iso- $B_p$  and iso- $P_i$  lines. Therefore, for any arbitrary distributions of  $B_p$  and  $P_i$ , a seeming  $L_{sd,i} - t_{sd}$  anti-correlation can always be obtained, which is not surprising.

It is undoubtedly of more scientific significance to investigate the magnetic fields and spin periods of the SLSN magnetars, which can provide more intrinsic information. The magnetic field strength and initial spin period of a magnetar can be derived by

$$B_p = 2 \times 10^{14} L_{sd,i,47}^{-1/2} t_{sd,5}^{-1} \text{ G}, \quad (6)$$

<sup>7</sup> The energy injected into supernova ejecta from a magnetar is usually considered to be in the form of high-energy photons. As the expansion of the ejecta at late times, its optical depth for high-energy photons could decrease quickly, which leads a remarkable fraction of injected high-energy photons to leak from the ejecta (see Wang et al. 2015 and references therein). Therefore, the energy absorption efficiency is suppressed. Meanwhile, this leaked high-energy emission could provide a smoking-gun observational signature for the magnetar-engine model (e.g. Kotera et al. 2013), which is worth to be explored in current and future observations.

and

$$P_1 = 1.4 \times 10^{-3} L_{\text{sd},i,47}^{-1/2} t_{\text{sd},5}^{-1/2} \text{ s}. \quad (7)$$

Then, the obtained values of  $B_p$  and  $P_1$  of the SLSN magnetars are listed in Table 2 and exhibited in Figure 3. By using the MCLUST software implementation by Fraley & Raftery (2002)<sup>8</sup>, we fit the two-dimension distribution of the data in Figure 3 by the Gaussian mixture model with the number of components evaluated using the Bayesian information criterion. As a result, it is found that the data distribution can well be fitted by a mixture of two log-normal functions, as shown by the  $1 - \sigma$  and  $3 - \sigma$  contours in Figure 3. The centering parameter values of the two separated regions are  $\langle B_p \rangle_{\text{SLSN1}} = 9.2 \times 10^{13}$  G,  $\langle P_1 \rangle_{\text{SLSN1}} = 2.7$  ms and  $\langle B_p \rangle_{\text{SLSN2}} = 3.7 \times 10^{14}$  G,  $\langle P_1 \rangle_{\text{SLSN2}} = 4.0$  ms. To be specific, fittings to the histograms of  $\log B_p$  and  $\log P_1$  are respectively presented in the right and upper panels of Figure 3. It is indicated that the SLSN magnetars can empirically be divided into two subclasses by a separating field strength of  $2.2 \times 10^{14}$  G. In addition, we would like to mention that, if we arbitrarily model some SLSNe that are not included in our sample (e.g., CSS100217 and SN 2008am) by the magnetar model, then the inferred parameters would be found to be very far away from the  $3 - \sigma$  edge of the above two log-Gaussians. This indicates that these excluded SLSNe are indeed not powered by a magnetar.

As another typical type of engine-driven phenomena, many GRBs have been suggested to harbor a magnetar engine too (Usov 1992; Duncan & Thompson 1992; Dai & Lu 1998a,b; Wheeler et al. 2000; Zhang & Meszaros 2001; Thompson et al. 2004; Metzger et al. 2011), which is strongly supported by the shallow-decay or plateau afterglows of GRBs (Yu et al. 2010; Rowlinson et al. 2013; Yi et al. 2014; Lü & Zhang 2014) and the rapidly rising and declining X-ray flares (Burrows et al. 2005; Dai et al. 2006; Wang & Dai 2013; Yi et al. 2016). In view of the same massive-star-collapse origin of long GRBs, it is obviously of great importance to compare the magnetar properties of SLSNe with those of long GRBs, which is one of the primary purposes of this paper. Such a comparison is exhibited in Figure 4, where the parameters of GRB magnetars are taken from the gold and silver samples in Lü & Zhang (2014)<sup>9</sup>. As shown, on one hand, the initial spin periods of GRB magnetars are generally concentrated within the range from about 1 ms to 10 ms, which is similar to the case of SLSN magnetars but has a relatively longer average value of  $\langle P_1 \rangle_{\text{GRB}} = 7.8$  ms. On the other hand, the magnetic field strengths of GRB magnetars, of an average value of  $\langle B_p \rangle_{\text{GRB}} = 6.3 \times 10^{15}$  G, are about several tens of times higher than those of SLSN magnetars. The dividing line between GRBs and SLSNe can roughly be set at a field strength of  $\sim 4 \times 10^{14}$  G, which is about ten times of the lower boundary of field strengths of SLSN magnetars. This significant difference in magnetic fields may arise from intrinsically different

natures (e.g., neutron stars, hybrid stars, quark stars, etc.) of the two types of magnetars. It is also suggested that ultrahigh magnetic fields could play a crucial role in producing GRBs. Figure 4 also reveals that the magnetic field strengths and initial spin periods of the two types of magnetars could satisfy two similar rough correlations, i.e.,  $B_p \sim 7.6 \times 10^{13} P_{i,-3}^{0.6}$  for SLSN magnetars and  $B_p \sim 8.3 \times 10^{14} P_{i,-3}^{0.8}$  for GRB magnetars. If these correlations are true, then we could conclude that the rotational energy of a newborn magnetar, no matter which kind of material it consists of, is always approximately inversely proportional to its magnetic energy, but with a large error. This could provide a clue to explore the dynamo of magnetars.

#### 4.2. Explosion parameters

The accumulated distribution of ejecta masses of the SLSNe is plotted in Figure 5. For a comparison, the distributions of GRB-associated hypernovae, normal Ic-BL supernovae that are unassociated with GRBs, and normal Ib/c supernovae are also presented, the data of which are taken from Cano et al. (2016) and Lyman et al. (2014). As shown, the mass range of SLSN ejecta is mainly from  $\sim 1M_\odot$  to  $\sim 10M_\odot$ , which is roughly consistent with the other types of supernovae. More specifically, the SLSN distribution seems broadly intermediate between those of normal supernovae and hypernovae, although larger numbers of the comparative supernovae are still needed for a more reliable comparison. The average ejecta masses of normal Ib/c supernovae, Ic-BL supernovae, SLSNe, and hypernovae are  $2.8M_\odot$ ,  $2.9M_\odot$ ,  $4.0M_\odot$ , and  $6.0M_\odot$ , respectively. On one hand, as argued by Nicholl et al. (2015a), this result may indicate that the ejecta masses could play the dominant role in distinguishing SLSNe as well as hypernovae from normal supernovae. On the other hand, in our opinion, these different mass distributions could be a consequence/indication of different central engines. One possibility is that the ejecta masses of SLSNe and hypernovae were all overestimated, since an isotropic geometry was always considered in calculations whereas the actual geometries of the ejecta are probably very anisotropic.

Figure 5 also shows that the ejecta masses of about 16% SLSNe are less than  $\sim 1M_\odot$ , which could indicate that these SLSNe originate from extremely-stripped progenitors but still might cause some concerns about their energy supplies and velocities. Nevertheless, in the magnetar model, the radiated energy of these SLSNe is provided by the magnetar engine, which is therefore irrelevant to the ejecta mass. In fact, even for much smaller ejecta of masses  $\sim 10^{-3} - 10^{-2}M_\odot$ , some analogous luminous transients have been suggested by Yu et al. (2013, 2015) for the systems of double neutron star mergers or accretion-induced collapses of white dwarfs. In these cases, the ejecta could be accelerated to an extremely high velocity. Then, would such high velocities also be predicted for low-mass SLSNe? In order to answer this question, we display the ejecta masses of SLSNe against the rotational energy of their remnant magnetars in Figure 6, which exhibits a correlation as

$$E_{\text{rot}} = 8.5 \times 10^{50} (M_{\text{ej}}/M_\odot)^{0.86} \text{ erg}, \quad (8)$$

where the rotational energy is calculated by  $E_{\text{rot}} =$

<sup>8</sup> <http://www.stat.washington.edu/raftery/Research/mbc.html>

<sup>9</sup> The derivation of the parameters of GRB magnetars is dependent on the measurements of jet beaming angles, since the energy release from a GRB magnetar is probably highly collimated (see Lü & Zhang 2014 for detailed discussions). Moreover, the assignment of the magnetar energy to GRB prompt emission, afterglow emission, and associated hypernova emission also needs to be analyzed carefully.

$L_{\text{sd},i}t_{\text{sd}}$ . By according to  $v_f \lesssim (2E_{\text{rot}}/M_{\text{ej}})^{1/2}$ , the final velocity of SLSN ejecta can be found to be not much higher than  $\sim 10^9 \text{ cm s}^{-1}$ , which is consistent with SLSN observations. This result is insensitive to the ejecta mass.

For a comparison, the masses and kinetic energies of the ejecta of hypernovae as well as some normal Ic-BL supernovae are also presented in Figure 6. We find with great interest that these hypernovae/Ic-BL supernovae data could follow an  $E_{\text{kin}} - M_{\text{ej}}$  relationship similar to the SLSN  $E_{\text{rot}} - M_{\text{ej}}$  relationship. In our opinion, the ejecta kinetic energy of a hypernova/Ic-BL supernova is ultimately provided by its central engine. Here the ultrahigh kinetic energies of some hypernovae on the order of  $\sim 10^{52} - 10^{53} \text{ erg}$  could be a problem for the magnetar engine model. Nevertheless, as suspected above, these kinetic energies could be somewhat overestimated due to the neglecting of the high anisotropy of hypernovae. Furthermore, in principle, an upper limit of several times  $10^{52} \text{ erg}$  on the rotational energy of a magnetar could still be acceptable, by considering of the possible differential rotation and uncertain equations of state of the magnetar. After all, the physical nature of the magnetars in hypernovae could be completely different from SLSN magnetars, as inferred by the magnetic field statistics in Section 4.1. In summary, the consistency between the possible  $E_{\text{rot}}(E_{\text{kin}}) - M_{\text{ej}}$  relationships of SLSNe and hypernovae/Ic-BL supernovae suggests that millisecond magnetars could also be the central engines of hypernovae/Ic-BL supernovae. However, different from SLSNe, the energy released from the magnetars of hypernovae/Ic-BL supernovae is mainly used to accelerate the ejecta rather than to power the supernova emission.

Finally, we would like to connect the  $E_{\text{rot}} - M_{\text{ej}}$  relationship with the work of Chen et al. (2016a) who suggested a possible correlation between the initial spin periods of SLSN magnetars and the metallicities of their host galaxies, although, which still needs to be examined by a much larger sample. In any case, theoretically, for a lower metallicity, the pre-explosion mass loss of a SLSN progenitor could be smaller and thus more angular momentum can be hold by the progenitor. As a result, more mass can be ejected during the supernova explosion and a more rapid rotating magnetar can be formed because its angular momentum is completely inherited from the core of the progenitor.

#### 4.3. Shapes of SLSN light curves

The shapes of SLSN light curves are usually treated as a preliminary basis to judge the possible properties of energy sources of the SLSNe. For example, some slowly-decaying SLSNe were usually ascribed to radioactive PISNe. In the framework of magnetar-powered supernovae, an approximative analytical solution of Equations (2–4) as presented in Yu et al. (2015) clearly shows that the basic shape of a light curve is mainly determined by the relationship between the spin-down timescale of the magnetar and the heat diffusion timescale of the supernova ejecta. To be specific, on one hand, a fast-evolving light curve can be obtained if  $t_{\text{sd}}$  and  $t_{\text{d}}$  are both short. On the other hand, for a relatively long  $t_{\text{d}}$  but  $t_{\text{sd}} \ll t_{\text{d}}$ , an exponentially fast-fading light curve can still be obtained. In other words, a fast-evolving light curve can always be produced with a short spin-down

timescale, which usually corresponds to a relatively high magnetic field. Therefore, it can be expected that the sharpness of SLSN light curves is tightly connected with the magnetic fields of their central magnetars.

For a direct description of light curve shapes, we define a rise timescale  $t_{\text{rise}}$  and a decline timescale  $t_{\text{dec}}$ , during which SLSN luminosity respectively increases from 10% of peak value to the peak and decreases from the peak to its 10%. We calculate these timescales with the model equations and the observationally-constrained model parameters, as listed in Table 3. Figure 7 shows that these two timescales are well correlated with each other with a ratio around  $t_{\text{dec}}/t_{\text{rise}} \sim (3 - 4)$ . Following Yu et al. (2015), the typical value of this ratio can be calculated by  $(1/\sqrt{0.1} - 1)/(1 - \sqrt{0.1}) = 3.2$ , by considering of the simplest form of light curves in the magnetar engine model, i.e.,  $L_{\text{sn}} \propto t^2$  for  $t < t_{\text{peak}}$  and  $L_{\text{sn}} \propto t^{-2}$  for  $t > t_{\text{peak}}$ , where  $t_{\text{peak}}$  is the peak time. A similar result had been presented in Nicholl et al. (2015a), where this  $t_{\text{rise}} - t_{\text{dec}}$  correlation was suggested to be an evidence for the magnetar engine model.

The sum of  $\Delta t_{10\%} = t_{\text{rise}} + t_{\text{dec}}$  can be used to define the width of the peak of light curves and furthermore to indicate the sharpness of light curves. As expected, Figure 8 indeed shows that the higher the magnetic fields, the smaller the light curve widths, which can be roughly expressed as  $\Delta t_{10\%} \propto B_p^{-0.68}$ . Therefore, by considering of the classification of SLSNe according to  $B_p$  as found in Section 4.1, it is natural to expect that SLSN light curves can also be divided into two types by a rough dividing line of  $\Delta t_{10\%} \sim 100 \text{ day}$  corresponding to  $B_p \sim 2.2 \times 10^{14} \text{ G}$ . Following such a criteria, we can successfully classify the fast-evolving (high-field) and slow-evolving (low-field) SLSN light curves into the left and right panels of Figure 9, respectively.

#### 5. DISCUSSIONS ON MAGNETAR-DRIVEN EXPLOSIONS

It has been widely discovered in observations that SLSNe have some similarities and even intrinsic connections with long GRBs and their associated hypernovae (van den Heuvel et al. 2013; Lunnan et al. 2015; Nicholl et al. 2015a; Yu & Li 2016; Inserra et al. 2016b; Japelj et al. 2016; Prajs et al. 2017). In particular, the host galaxies of GRBs and SLSNe I are found to share many common properties (e.g. high star formation rate and low metallicity; Lunnan et al. 2014), although some (not surprising) differences still exist (Angus et al. 2016). More directly, a SLSNe (i.e., SN 2011kl) was even discovered in the afterglow emission of GRB 111209A (Levan et al. 2013; Greiner et al. 2015).

From a theoretical point of view, the most fundamental connection between SLSNe and GRBs is that both of these two types of stellar explosions could leave a remnant millisecond magnetar, although it can not be ruled out that some other energy sources could be responsible for a fraction of SLSNe (e.g., interaction-powered SLSNe) and GRBs (e.g. black hole accretion-driven GRBs). Besides to contribute a useful continuous energy supply, a magnetar engine can also be employed to effectively explain the intermittent flare activities discovered in both GRB afterglow emission (Dai et al. 2006) and SLSN emission (Yu & Li 2016). This united magnetar engine model for both SLSNe and GRBs implies that these two explosion phenomena probably have very similar progen-

itors, environments, and even explosion processes. Meanwhile, differences between their progenitors must also be remarkable, which is needed to explain the completely different magnetic fields of their remnant magnetars. In Figure 10, we illustrate our preliminary consideration of a possible physical classification of various stellar explosions in the united magnetar engine model, as discussed as follows.

First of all, the magnetic fields of SLSN magnetars are nearly all higher than a lower limit value that is around the Landau critical field of electrons as  $B_c = m_e^2 c^3 / (q \hbar) = 4.4 \times 10^{13}$  G, where  $m_e$  and  $q$  are the mass and charge of electrons and  $\hbar$  is the reduced Planck constant. Such a field boundary of clear physical meaning might not just be a coincidence. For a magnetar of a supercritical magnetic field, it might have some unique properties making the magnetar physically different from normal pulsars, because the Landau quantization of electrons can make the phase space of the electrons very anisotropic. Therefore, we suspect that a supercritical magnetic field could play a fundamental role in SLSN explosions, besides to determine a spin-down timescale comparable to the heat diffusion timescale of supernova ejecta.

While the magnetic fields of SLSN magnetars are mainly within the range of  $\sim (1-10)B_c$ , GRB magnetars are generally found to own a field higher than  $\sim 10B_c$ . In our opinion, these completely different ranges of magnetic fields may be intrinsically determined by the different interior ingredients of SLSN magnetars and GRB magnetars, although their dynamo processes could still be common as indicated by the similar rough  $B_p - P_i$  relationships. The possible consequences of the ultrahigh magnetic fields of GRB magnetars are of more interests here. For the field range of  $\sim (10-300)B_c$ , the number of electron Landau levels is only several tens and even a few (e.g. Zheng & Yu 2006), in which cases electrons would behavior very close to a one-dimension gas. As a result, some processes (e.g. neutrino emission) of GRB magnetars must be dominated in the magnetic field direction and thus the resulted hypernovae could be highly anisotropic as considered in Section 4.2.

The ultrahigh magnetic field of a GRB magnetar could play a crucial role in the formation and collimation of a relativistic jet, by coupling with a highly anisotropic neutrino wind during the first  $\sim 10-100$  s (Metzger et al. 2011). During this phase, the propeller effect of possible fallback accretion could also play a part and extract the rotational energy of the magnetar. Subsequently, during a relatively longer but still very short timescale of  $\sim 10^{2-4}$  s, the ultrahigh magnetic field can further lead the magnetar to release its remaining rotational energy, a fraction of which can contribute to a plateau component to the GRB afterglow emission (Yu et al. 2010). At the same time, a comparable amount of energy could be injected into the supernova ejecta in a timescale that is significantly shorter than the diffusion timescale of months. As a result, the supernova ejecta will be accelerated quickly and significantly and the resulted hypernovae should own a broad-line featured spectrum. However, the hypernova luminosity can not be effectively enhanced, because the injected energy has been consumed much earlier than the supernova emission. These characteristics have been widely confirmed

by hypernova observations (Galama et al. 1998; Hjorth et al. 2003; Stanek et al. 2003). Furthermore, the kinetic energy of hypernovae can basically reflect the total rotational energy of magnetars, as we discussed on Figure 6.

While a magnetic field of  $\sim (1-10)B_c$  is benefit for producing an unusual bright supernova emission, a field higher than  $\sim 10B_c$  could be indispensable for jet formation. Therefore, it could be natural to conclude that GRB-SLSN associations can only appear for magnetar engines of a magnetic field around  $\sim 10B_c$ . It is found that the magnetar engine of SN 2011kl indeed satisfies this condition. However, for this case, the problem is that the magnetic field derived from the afterglow of GRB 111209A is inconsistent with that derived from SN 2011kl (Kann et al. 2016). In any case, the present reported SLSN-associated GRBs are all ultra-long GRBs, which might have a progenitor completely different from those of typical long GRBs. Then, it can not be ruled out that these SLSNe have a unique origin. For example, Nakauchi et al. (2013) suggested these SLSNe to be contributed by a jet cocoon that breaks out from a blue supergiant.

A remaining question is that what the nature of normal Ic-BL supernovae, which are unassociated with GRBs. In view of their high similarity with hypernovae, the most straightforward answer is to connect them with magnetars of ultrahigh magnetic fields. However, in this case, a further question would arise as that what suppresses the formation of relativistic jets. Therefore, we prefer to suggest that normal Ic-BL supernovae could be driven by magnetars similar to SLSN ones. The difference is that fallback accretion could take place for normal Ic-BL supernovae, as proposed by Piro & Ott (2011). The high magnetic field of a magnetar can lead the accretion to quickly enter into a propeller phase. Then most rotational energy of the magnetar is extracted by the propeller outflow during a very short timescale. As a result, the supernova ejecta is accelerated but the supernova emission is still powered by radioactivities, which is similar to the hypernova cases.

As discussed, no matter which types of millisecond magnetars are formed, the ejecta of all magnetar-driven supernovae including SLSNe, hypernovae, and normal Ic-BL supernovae should eventually be accelerated to a high speed. Therefore, as long as these explosions happen in a dense environment, a strong shock emission can always arise and provide a substantial and even dominative contribution to the supernova emission, i.e., an interaction-powered SLSN could be generated. For example, an interaction signature of narrow lines could finally appear at a few hundreds of days after peak emission for some broad-lined SLSNe II (e.g. 2013hx). It is further suspected that, even for SLSN IIn, their strong interactions could also ultimately be resulted from the powering of a magnetar engine. The intrinsic differences between SLSNe I and II could be not primarily determined by their energy engines, but be a reflection of their different environments and host galaxies.

Finally, in view of the wide and significant influences of millisecond magnetars on the various unusual supernova phenomena, it can be enlightened that some ordinary supernova emission could also be partially powered or aided by a pulsar engine, even though the magnetic field

of the pulsar is normal (e.g. Li et al. 2015 for SN 1054). This idea could be supported by the wide existences of engine-driven jets in the remnants of many ordinary core-collapse supernovae (Bear & Soker 2016a,b).

## 6. SUMMARY AND CONCLUSION

By considering of that the majority of observed SLSNe are powered by continuous energy injection from a magnetar engine, we fit the bolometric light curves of 27 SLSNe I and 4 SLSNe II without narrow-line features. As a result, we obtain the basic parameters of these SLSNe including their ejecta masses and the initial spin periods and magnetic field strengths of remnant magnetars. The primary ranges of these parameters are found to be  $\sim (1 - 10)M_{\odot}$ ,  $\sim (1 - 10)$  ms, and  $\sim (1 - 10)B_c$ , respectively, with average values of  $4.0M_{\odot}$ , 3.5ms, and  $2.0 \times 10^{14}$  G, by assuming  $\kappa = 0.1\text{cm}^2\text{g}^{-1}$ . In more details, SLSN magnetars can be divided into two subclasses by a magnetic field strength of  $\sim 2.2 \times 10^{14}$  G. Furthermore, the bolometric light curves being fast-evolving and slow-evolving in observations are found to be tightly connected with these high- and low-field subclasses of magnetars, respectively.

By connecting with long GRBs and their associated hypernovae, it is suggested that high magnetic fields of magnetars could play a crucial role in distinguishing hypernovae and SLSNe from normal supernovae and even

in distinguishing themselves. As a possible consequence, the high magnetic fields could cause an anisotropic geometry of the supernovae and even lead to the formation of a highly beamed jet. Therefore, on one hand, it is of great importance to investigate in future the possible influences of high magnetic fields on the behaviors of newly-born millisecond magnetars, the knowledge of which is very limited now. On the other hand, it is also important to explore the physical reasons being responsible for the formation of the high magnetic fields. Fall-back accretions with different accretion rates could play a part in these processes.

Besides the common magnetar engines, the connection between SLSNe and long GRBs could also be exhibited in the distributions of their ejecta masses. In particular, the possible correlations between magnetar properties and ejecta masses as well as metallicities of host galaxies (Chen et al. 2016a) could provide a very important clue to explore the nature of the progenitors of these stellar explosions.

The authors acknowledge Z. G. Dai for his useful discussions. This work is supported by the National Natural Science Foundation of China (grant No. 11473008) and the Program for New Century Excellent Talents in University (grant No. NCET-13-0822).

## REFERENCES

- Angus, C. R., Levan, A. J., Perley, D. A., et al. 2016, *MNRAS*, 458, 84
- Arnett, W. D. 1982, *ApJ*, 253, 785
- Barkat, Z., Rakavy, G., & Sack, N. 1967, *Physical Review Letters*, 18, 379
- Bear, E., & Soker, N. 2016, arXiv:1611.07327
- Bear, E., & Soker, N. 2016, arXiv:1606.08149
- Benetti, S., Nicholl, M., Cappellaro, E., et al. 2014, *MNRAS*, 441, 289
- Burrows, D. N., Romano, P., Falcone, A., et al. 2005, *Science*, 309, 1833
- Cano, Z., Wang, S.-Q., Dai, Z.-G., & Wu, X.-F. 2016, *LPI Contributions*, 1962, 4116
- Chatzopoulos, E., & Wheeler, J. C. 2012, *ApJ*, 760, 154
- Chatzopoulos, E., Wheeler, J. C., Vinko, J., Horvath, Z. L., & Nagy, A. 2013, *ApJ*, 773, 76
- Chen, K.-J., Woosley, S. E., & Sukhbold, T. 2016b, *ApJ*, 832, 73
- Chen, T.-W., Nicholl, M., Smartt, S. J., et al. 2016c, arXiv:1611.09910
- Chen, T.-W., Smartt, S. J., Jerkstrand, A., et al. 2015, *MNRAS*, 452, 1567
- Chen, T.-W., Smartt, S. J., Yates, R. M., et al. 2016a, arXiv:1605.04925
- Chen, T.-W., Smartt, S. J., Bresolin, F., et al. 2013, *ApJ*, 763, L28
- Chevalier, R. A., & Irwin, C. M. 2011, *ApJ*, 729, L6
- Chomiuk, L., Chornock, R., Soderberg, A. M., et al. 2011, *ApJ*, 743, 114
- Chornock, R., Berger, E., Rest, A., et al. 2013, *ApJ*, 767, 162
- Dai, Z. G., & Lu, T. 1998, *Physical Review Letters*, 81, 4301
- Dai, Z. G., & Lu, T. 1998, *A&A*, 333, L87
- Dai, Z. G., Wang, S. Q., Wang, J. S., Wang, L. J., & Yu, Y. W. 2016, *ApJ*, 817, 132
- Dai, Z. G., Wang, X. Y., Wu, X. F., & Zhang, B. 2006, *Science*, 311, 1127
- Dainotti, M. G., Cardone, V. F., & Capozziello, S. 2008, *MNRAS*, 391, L79
- Dessart, L., Hillier, D. J., Waldman, R., Livne, E., & Blondin, S. 2012, *MNRAS*, 426, L76
- Dexter, J., & Kasen, D. 2013, *ApJ*, 772, 30
- Dong, S., Shappee, B. J., Prieto, J. L., et al. 2016, *Science*, 351, 257
- Duncan, R. C., & Thompson, C. 1992, *ApJ*, 392, L9
- Fraleigh, C. & Raftery, A. E. 2002, *Journal of the American Statistical Association*, 97, 611
- Gal-Yam, A., Mazzali, P., Ofek, E. O., et al. 2009, *Nature*, 462, 624
- Gal-Yam, A. 2012, *Science*, 337, 927
- Galama, T. J., Vreeswijk, P. M., van Paradijs, J., et al. 1998, *Nature*, 395, 670
- Gezari, S., Halpern, J. P., Grupe, D., et al. 2009, *ApJ*, 690, 1313
- Ginzburg, S., & Balberg, S. 2012, *ApJ*, 757, 178
- Godoy-Rivera, D., Stanek, K. Z., Kochanek, C. S., et al. 2017, *MNRAS*,
- Greiner, J., Mazzali, P. A., Kann, D. A., et al. 2015, *Nature*, 523, 189
- Heger, A., & Woosley, S. E. 2002, *ApJ*, 567, 532
- Hjorth, J., Sollerman, J., Møller, P., et al. 2003, *Nature*, 423, 847
- Howell, D. A., Kasen, D., Lidman, C., et al. 2013, *ApJ*, 779, 98
- Inserra, C., Bulla, M., Sim, S. A., & Smartt, S. J. 2016a, *ApJ*, 831, 79
- Inserra, C., Smartt, S. J., Gall, E. E. E., et al. 2016b, arXiv:1604.01226
- Inserra, C., Smartt, S. J., Jerkstrand, A., et al. 2013, *ApJ*, 770, 128
- Japelj, J., Vergani, S. D., Salvaterra, R., Hunt, L. K., & Mannucci, F. 2016, *A&A*, 593, A115
- Kann, D. A., Schady, P., Olivares E., F., et al. 2016, arXiv:1606.06791
- Kasen, D., & Bildsten, L. 2010, *ApJ*, 717, 245
- Kasen, D., Metzger, B. D., & Bildsten, L. 2016, *ApJ*, 821, 36
- Kotera, K., Phinney, E. S., & Olinto, A. V. 2013, *MNRAS*, 432, 3228
- Kozyreva, A., & Blinnikov, S. 2015, *MNRAS*, 454, 4357
- Lü, H.-J., & Zhang, B. 2014, *ApJ*, 785, 74
- Lü, H.-J., Zhang, B., Lei, W.-H., Li, Y., & Lasky, P. D. 2015, *ApJ*, 805, 89
- Leloudas, G., Fraser, M., Stone, N. C., et al. 2016, *Nature Astronomy*, 1, 0002
- Leloudas, G., Schulze, S., Krühler, T., et al. 2015, *MNRAS*, 449, 917

- Levan, A. J., Read, A. M., Metzger, B. D., Wheatley, P. J., & Tanvir, N. R. 2013, *ApJ*, 771, 136
- Li, S.-Z., Yu, Y.-W., & Huang, Y. 2015, *Research in Astronomy and Astrophysics*, 15, 1823
- Lunnan, R., Chornock, R., Berger, E., et al. 2013, *ApJ*, 771, 97
- Lunnan, R., Chornock, R., Berger, E., et al. 2016, *ApJ*, 831, 144
- Lunnan, R., Chornock, R., Berger, E., et al. 2015, *ApJ*, 804, 90
- Lyman, J. D., Bersier, D., & James, P. A. 2014, *MNRAS*, 437, 3848
- Margutti, R., Metzger, B. D., Chornock, R., et al. 2016, *arXiv:1610.01632*
- McCrum, M., Smartt, S. J., Kotak, R., et al. 2014, *MNRAS*, 437, 656
- Metzger, B. D., Giannios, D., Thompson, T. A., Bucciantini, N., & Quataert, E. 2011, *MNRAS*, 413, 2031
- Miller, A. A., Chornock, R., Perley, D. A., et al. 2009, *ApJ*, 690, 1303
- Moriya, T., Tominaga, N., Blinnikov, S. I., Baklanov, P. V., & Sorokina, E. I. 2011, *MNRAS*, 415, 199
- Moriya, T. J., Blinnikov, S. I., Tominaga, N., et al. 2013, *MNRAS*, 428, 1020
- Moriya, T. J., Chen, T.-W., & Langer, N. 2016, *arXiv:1612.06917*
- Nakauchi, D., Kashiyama, K., Suwa, Y., & Nakamura, T. 2013, *ApJ*, 778, 67
- Neill, J. D., Sullivan, M., Gal-Yam, A., et al. 2011, *ApJ*, 727, 15
- Nicholl, M., Berger, E., Smartt, S. J., et al. 2016, *ApJ*, 826, 39
- Nicholl, M., Smartt, S. J., Jerkstrand, A., et al. 2014, *MNRAS*, 444, 2096
- Nicholl, M., Smartt, S. J., Jerkstrand, A., et al. 2013, *Nature*, 502, 346
- Nicholl, M., Smartt, S. J., Jerkstrand, A., et al. 2015a, *MNRAS*, 452, 3869
- Nicholl, M., Smartt, S. J., Jerkstrand, A., et al. 2015b, *ApJ*, 807, L18
- Ofek, E. O., Cameron, P. B., Kasliwal, M. M., et al. 2007, *ApJ*, 659, L13
- Ostriker, J. P., & Gunn, J. E. 1971, *ApJ*, 164, L95
- Papadopoulos, A., D'Andrea, C. B., Sullivan, M., et al. 2015, *MNRAS*, 449, 1215
- Pastorello, A., Smartt, S. J., Botticella, M. T., et al. 2010, *ApJ*, 724, L16
- Perley, D. A., Quimby, R. M., Yan, L., et al. 2016, *ApJ*, 830, 13
- Piro, A. L., & Ott, C. D. 2011, *ApJ*, 736, 108
- Prajs, S., Sullivan, M., Smith, M., et al. 2017, *MNRAS*, 464, 3568
- Quimby, R. M., Kulkarni, S., Ofek, E., et al. 2010, *The Astronomer's Telegram*, 2740,
- Quimby, R. M., Kulkarni, S. R., Kasliwal, M. M., et al. 2011, *Nature*, 474, 487
- Quimby, R. M., Aldering, G., Wheeler, J. C., et al. 2007, *ApJ*, 668, L99
- Quimby, R. M., Oguri, M., More, A., et al. 2014, *Science*, 344, 396
- Rowlinson, A., Gompertz, B. P., Dainotti, M., et al. 2014, *MNRAS*, 443, 1779
- Rowlinson, A., O'Brien, P. T., Metzger, B. D., Tanvir, N. R., & Levan, A. J. 2013, *MNRAS*, 430, 1061
- Smith, M., Sullivan, M., D'Andrea, C. B., et al. 2016, *ApJ*, 818, L8
- Smith, N., Li, W., Foley, R. J., et al. 2007, *ApJ*, 666, 1116
- Smith, N., & McCray, R. 2007, *ApJ*, 671, L17
- Stanek, K. Z., Matheson, T., Garnavich, P. M., et al. 2003, *ApJ*, 591, L17
- Thompson, T. A., Chang, P., & Quataert, E. 2004, *ApJ*, 611, 380
- Umeda, H., & Nomoto, K. 2008, *ApJ*, 673, 1014-1022
- Usov, V. V. 1992, *Nature*, 357, 472
- van den Heuvel, E. P. J., & Portegies Zwart, S. F. 2013, *ApJ*, 779, 114
- Vreeswijk, P. M., Savaglio, S., Gal-Yam, A., et al. 2014, *ApJ*, 797, 24
- Wang, F. Y., & Dai, Z. G. 2013, *Nature Physics*, 9, 465
- Wang, S. Q., Liu, L. D., Dai, Z. G., Wang, L. J., & Wu, X. F. 2016, *ApJ*, 828, 87
- Wang, S. Q., Wang, L. J., Dai, Z. G., & Wu, X. F. 2015, *ApJ*, 799, 107
- Wheeler, J. C., Yi, I., Höflich, P., & Wang, L. 2000, *ApJ*, 537, 810
- Woosley, S. E. 2010, *ApJ*, 719, L204
- Woosley, S. E., Blinnikov, S., & Heger, A. 2007, *Nature*, 450, 390
- Yan, L., Quimby, R., Gal-Yam, A., et al. 2016, *arXiv:1611.02782*
- Yan, L., Quimby, R., Ofek, E., et al. 2015, *ApJ*, 814, 108
- Yi, S. X., Dai, Z. G., Wu, X. F., & Wang, F. Y. 2014, *arXiv:1401.1601*
- Yi, S.-X., Xi, S.-Q., Yu, H., et al. 2016, *ApJS*, 224, 20
- Yu, Y.-W., Cheng, K. S., & Cao, X.-F. 2010, *ApJ*, 715, 477
- Yu, Y.-W., Zhang, B., & Gao, H. 2013, *ApJ*, 776, L40
- Yu, Y.-W., & Li, S.-Z. 2016, *arXiv:1607.00626*
- Yu, Y.-W., Li, S.-Z., & Dai, Z.-G. 2015, *ApJ*, 806, L6
- Zhang, B., & Mészáros, P. 2001, *ApJ*, 552, L35
- Zheng, X. P., & Yu, Y. W. 2006, *A&A*, 445, 627



TABLE 1  
OBSERVATIONAL INFORMATION OF SLSNE

SLSNe	Types	R.A.	Decl.	$z$	References
CSS121015	II	00 <sup>h</sup> 42 <sup>m</sup> 44 <sup>s</sup> .38	+13°28′26″.197	0.2868	Benetti+2014
DES13S2cmm	I	02 <sup>h</sup> 42 <sup>m</sup> 32 <sup>s</sup> .82	−01°21′30″.1	0.663	Papadopoulos+2015
DES14X3taz	I	02 <sup>h</sup> 28 <sup>m</sup> 04 <sup>s</sup> .46	−04°05′12″.7	0.608	Smith+2016
Gaia16apd	I	12 <sup>h</sup> 02 <sup>m</sup> 51 <sup>s</sup> .71	+44°15′27″.40	0.1018	Yan+2016; Nicholl+2016
iPTF13ajg	I	16 <sup>h</sup> 39 <sup>m</sup> 03 <sup>s</sup> .95	+37°01′38″.4	0.7403	Vreeswijk+2014
iPTF13ehe	I	06 <sup>h</sup> 53 <sup>m</sup> 21 <sup>s</sup> .50	+67°07′56″.0	0.3434	Yan+2015; Wang+2016
LSQ12dlf	I	01 <sup>h</sup> 50 <sup>m</sup> 29 <sup>s</sup> .8	−21°48′45″.4	0.255	Nicholl+2014
LSQ14bdq	I	10 <sup>h</sup> 01 <sup>m</sup> 41 <sup>s</sup> .60	−12°22′13″.4	0.345	Nicholl+2015
LSQ14mo	I	10 <sup>h</sup> 22 <sup>m</sup> 41 <sup>s</sup> .53	−16°55′14″.4	0.2563	Chen+2016
PS1−10awh	I	22 <sup>h</sup> 14 <sup>m</sup> 29 <sup>s</sup> .831	−00°04′03″.62	0.908	Chomiuk+2011
PS1−10bzj	I	03 <sup>h</sup> 31 <sup>m</sup> 39 <sup>s</sup> .862	−27°47′42″.17	0.650	Lunnan+2013
PS1−11ap	I	10 <sup>h</sup> 48 <sup>m</sup> 27 <sup>s</sup> .73	+57°09′09″.2	0.524	McCrum+2014
PS1−14bj	I	10 <sup>h</sup> 02 <sup>m</sup> 08 <sup>s</sup> .433	+03°39′19″.02	0.5215	Lunnan+2016
PS15br	II	11 <sup>h</sup> 25 <sup>m</sup> 19 <sup>s</sup> .22	+08°14′18″.9	0.101	Inserra+2016
PTF10hgi	I	16 <sup>h</sup> 37 <sup>m</sup> 47 <sup>s</sup> .08	+06°12′32″.35	0.100	Inserra+2013
PTF11rks	I	01 <sup>h</sup> 39 <sup>m</sup> 45 <sup>s</sup> .49	+29°55′26″.87	0.190	Inserra+2013
PTF12dam	I	14 <sup>h</sup> 24 <sup>m</sup> 46 <sup>s</sup> .20	+46°13′48″.3	0.107	Chen+2015
SCP06F6	I	14 <sup>h</sup> 32 <sup>m</sup> 27 <sup>s</sup> .395	+33°32′24″.83	1.189	Berkeley+2009; Quimby+2011; Chatzopoulos+2013
SN 2005ap	I	13 <sup>h</sup> 01 <sup>m</sup> 14 <sup>s</sup> .83	+27°43′32″.3	0.2832	Quimby+2007; Chatzopoulos+2013
SN 2007bi	I	13 <sup>h</sup> 19 <sup>m</sup> 20 <sup>s</sup> .2	+08°55′44″.0	0.1279	Gal-Yam+2009; Chatzopoulos+2013
SN 2008es	II	11 <sup>h</sup> 56 <sup>m</sup> 49 <sup>s</sup> .06	+54°27′25″.77	0.213	Miller+2009; Gezari+2009; Chatzopoulos+2013
SN 2010gx	I	11 <sup>h</sup> 25 <sup>m</sup> 46 <sup>s</sup> .71	−08°49′41″.4	0.23	Pastorello+2010
SN 2010kd	I	12 <sup>h</sup> 08 <sup>m</sup> 01 <sup>s</sup> .11	+49°13′31″.1	0.101	Chatzopoulos+2013
SN 2011ke	I	13 <sup>h</sup> 50 <sup>m</sup> 57 <sup>s</sup> .78	+26°16′42″.40	0.143	Inserra+2013
SN 2011kf	I	14 <sup>h</sup> 36 <sup>m</sup> 57 <sup>s</sup> .53	+16°30′56″.6	0.245	Drake+2012; Inserra+2013
SN 2011kl	I	00 <sup>h</sup> 57 <sup>m</sup> 22 <sup>s</sup> .64	−46°48′03″.6	0.677	Greiner+2015
SN 2012il	I	09 <sup>h</sup> 46 <sup>m</sup> 12 <sup>s</sup> .91	+19°50′28″.70	0.175	Inserra+2013
SN 2013dg	I	13 <sup>h</sup> 18 <sup>m</sup> 41 <sup>s</sup> .38	−07°04′43″.1	0.265	Nicholl+2014
SN 2013hx	II	01 <sup>h</sup> 35 <sup>m</sup> 32 <sup>s</sup> .83	−57°57′50″.6	0.125	Inserra+2016
SN 2015bn	I	11 <sup>h</sup> 33 <sup>m</sup> 41 <sup>s</sup> .55	+00°43′33″.4	0.1136	Nicholl+2016
SSS120810	I	23 <sup>h</sup> 18 <sup>m</sup> 01 <sup>s</sup> .8	−56°09′25″.6	0.156	Nicholl+2014

TABLE 2  
THE VALUES OF MODEL PARAMETERS

SLSN	$M_{\text{ej}}/M_{\odot}$	$L_{\text{sd},i}/10^{45}\text{erg s}^{-1}$	$t_{\text{sd}}/\text{day}$	$B_{\text{p}}/10^{13}\text{G}$	$P_{\text{i}}/\text{ms}$	$E_{\text{rot}}/10^{50}\text{erg}$
CSS121015	$2.51 \pm 0.27$	$3.99 \pm 1.12$	$9.82 \pm 1.94$	$11.80 \pm 2.33$	$2.43 \pm 0.58$	$33.88 \pm 16.18$
DES13S2cmm	$0.90 \pm 0.08$	$0.10 \pm 0.01$	$91.03 \pm 12.56$	$7.99 \pm 1.10$	$5.01 \pm 0.57$	$7.97 \pm 1.82$
DES14X3taz	$6.40 \pm 2.15$	$4.00 \pm 2.47$	$14.53 \pm 4.93$	$7.97 \pm 2.71$	$2.00 \pm 0.96$	$50.16 \pm 48.02$
Gaia16apd	$3.65 \pm 0.53$	$5.68 \pm 2.19$	$9.55 \pm 2.47$	$10.17 \pm 2.63$	$2.07 \pm 0.66$	$46.88 \pm 30.18$
iPTF13ajp	$4.02 \pm 1.70$	$34.60 \pm 50.51$	$3.55 \pm 3.23$	$11.10 \pm 10.11$	$1.37 \pm 1.63$	$106.0 \pm 251.3$
iPTF13ehe	$6.79 \pm 4.26$	$0.79 \pm 1.16$	$43.02 \pm 52.01$	$6.07 \pm 7.34$	$2.62 \pm 3.52$	$29.18 \pm 78.39$
LSQ12df	$2.02 \pm 0.22$	$0.76 \pm 0.21$	$16.38 \pm 3.52$	$16.20 \pm 3.48$	$4.31 \pm 1.07$	$10.77 \pm 5.33$
LSQ14bdq	$14.98 \pm 0.90$	$9.75 \pm 1.38$	$11.00 \pm 0.96$	$6.74 \pm 0.59$	$1.47 \pm 0.17$	$92.63 \pm 21.15$
LSQ14mo	$1.35 \pm 0.08$	$2.09 \pm 0.41$	$5.34 \pm 2.33$	$29.98 \pm 13.10$	$4.55 \pm 1.44$	$9.64 \pm 6.09$
PS1-10awh	$2.52 \pm 0.47$	$5.08 \pm 2.53$	$7.03 \pm 2.31$	$14.60 \pm 4.80$	$2.55 \pm 1.05$	$30.86 \pm 25.86$
PS1-10bj	$2.28 \pm 0.38$	$16.23 \pm 1.00$	$1.58 \pm 0.57$	$36.39 \pm 13.02$	$3.01 \pm 1.46$	$22.15 \pm 21.57$
PS1-11ap	$2.42 \pm 0.15$	$0.52 \pm 0.07$	$24.72 \pm 2.58$	$12.94 \pm 0.14$	$4.23 \pm 0.50$	$11.18 \pm 2.63$
PS1-14bj	$17.89 \pm 2.43$	$0.79 \pm 0.28$	$36.32 \pm 8.73$	$7.19 \pm 1.73$	$2.85 \pm 0.85$	$24.67 \pm 14.85$
PS15br	$0.85 \pm 0.04$	$0.07 \pm 0.00$	$79.38 \pm 5.43$	$10.71 \pm 0.73$	$6.27 \pm 0.37$	$5.09 \pm 0.60$
PTF10hgi	$2.33 \pm 0.25$	$1.20 \pm 0.57$	$5.80 \pm 1.63$	$36.45 \pm 10.23$	$5.77 \pm 2.17$	$6.01 \pm 4.52$
PTF11rks	$0.83 \pm 0.25$	$0.26 \pm 0.22$	$12.06 \pm 8.32$	$37.37 \pm 25.76$	$8.53 \pm 6.45$	$2.75 \pm 4.16$
PTF12dam	$7.26 \pm 1.00$	$1.43 \pm 0.51$	$24.41 \pm 6.18$	$7.93 \pm 2.01$	$2.57 \pm 0.78$	$30.17 \pm 18.39$
SCP06F6	$2.86 \pm 2.53$	$0.95 \pm 1.74$	$36.91 \pm 61.10$	$6.23 \pm 10.01$	$2.53 \pm 4.34$	$31.30 \pm 107.5$
SN 2005ap	$0.81 \pm 0.14$	$0.94 \pm 0.25$	$31.44 \pm 6.87$	$7.66 \pm 2.47$	$2.81 \pm 0.81$	$25.30 \pm 14.64$
SN 2007bi	$5.99 \pm 0.77$	$0.90 \pm 0.25$	$31.44 \pm 6.87$	$7.77 \pm 1.70$	$2.87 \pm 0.73$	$24.36 \pm 12.43$
SN 2008es	$3.01 \pm 0.69$	$1.95 \pm 1.05$	$20.51 \pm 8.71$	$8.08 \pm 3.43$	$2.40 \pm 1.15$	$34.62 \pm 33.25$
SN 2010gx	$2.80 \pm 0.12$	$56.61 \pm 12.15$	$0.65 \pm 0.08$	$47.39 \pm 5.80$	$2.51 \pm 0.42$	$31.75 \pm 10.70$
SN 2010kd	$7.60 \pm 0.69$	$4.04 \pm 1.28$	$7.99 \pm 1.57$	$14.41 \pm 2.83$	$2.68 \pm 0.69$	$27.91 \pm 14.32$
SN 2011ke	$2.23 \pm 0.13$	$35.90 \pm 9.09$	$0.80 \pm 0.12$	$48.15 \pm 7.11$	$2.83 \pm 0.57$	$24.89 \pm 9.98$
SN 2011kf	$2.10 \pm 0.38$	$2141 \pm 1723$	$0.47 \pm 0.22$	$33.77 \pm 15.86$	$1.52 \pm 0.97$	$86.65 \pm 110.5$
SN 2011kl	$0.51 \pm 0.06$	$0.10 \pm 0.02$	$16.63 \pm 4.31$	$44.94 \pm 1.17$	$12.04 \pm 3.07$	$1.38 \pm 0.70$
SN 2012il	$1.60 \pm 0.42$	$2.29 \pm 2.02$	$4.29 \pm 2.39$	$35.71 \pm 19.87$	$4.86 \pm 3.50$	$8.47 \pm 12.20$
SN 2013dg	$1.76 \pm 0.12$	$2.53 \pm 0.64$	$4.08 \pm 0.67$	$35.69 \pm 5.83$	$4.74 \pm 0.99$	$8.91 \pm 3.73$
SN 2013hx	$3.47 \pm 0.33$	$7.24 \pm 1.82$	$7.29 \pm 1.20$	$11.79 \pm 1.94$	$2.09 \pm 0.43$	$45.64 \pm 18.96$
SN 2015bn	$5.28 \pm 0.28$	$1.07 \pm 0.10$	$42.09 \pm 3.11$	$5.32 \pm 0.39$	$2.27 \pm 0.19$	$38.90 \pm 6.55$
SSS120810	$5.59 \pm 0.94$	$66.09 \pm 58.26$	$1.09 \pm 0.55$	$26.24 \pm 13.27$	$1.80 \pm 1.25$	$61.97 \pm 85.96$

TABLE 3  
THE LIGHT CURVE PARAMETERS

SLSN	$\Delta t_{10\%}$	$t_{\text{rise}}$	$t_{\text{dec}}$
CSS121015	106.1	24.12	81.93
DES13S2cmm	278.7	23.40	255.3
DES14X3taz	183.8	43.08	140.7
Gaia16apd	121.4	28.58	92.82
iPTF13ajp	85.82	21.60	64.22
iPTF13ehe	308.1	60.97	247.1
LSQ12dlf	128.6	26.28	102.3
LSQ14bdq	245.4	61.04	184.4
LSQ14mo	70.66	16.53	54.12
PS1-10awh	95.79	22.75	73.03
PS1-10bjz	67.42	16.74	50.68
PS1-11ap	166.2	31.81	134.4
PS1-14bj	456.1	105.3	350.8
PS15br	249.3	22.13	227.2
PTF10hgi	100.1	24.02	76.06
PTF11rks	80.12	15.17	64.94
PTF12dam	249.5	55.58	194.0
SCP06F6	208.0	35.83	172.2
SN 2005ap	126.0	16.78	109.2
SN 2007bi	258.1	53.77	204.3
SN 2008es	154.8	31.50	123.3
SN 2010gx	65.06	15.64	50.32
SN 2010kd	185.0	45.76	139.3
SN 2011ke	60.06	14.51	45.54
SN 2011kf	43.34	10.44	32.90
SN 2011kl	79.28	12.20	67.08
SN 2012il	73.31	17.69	55.63
SN 2013dg	76.16	18.52	57.64
SN 2013hx	108.9	26.26	82.59
SN 2015bn	269.7	50.87	218.8
SSS120810	98.17	23.52	74.65

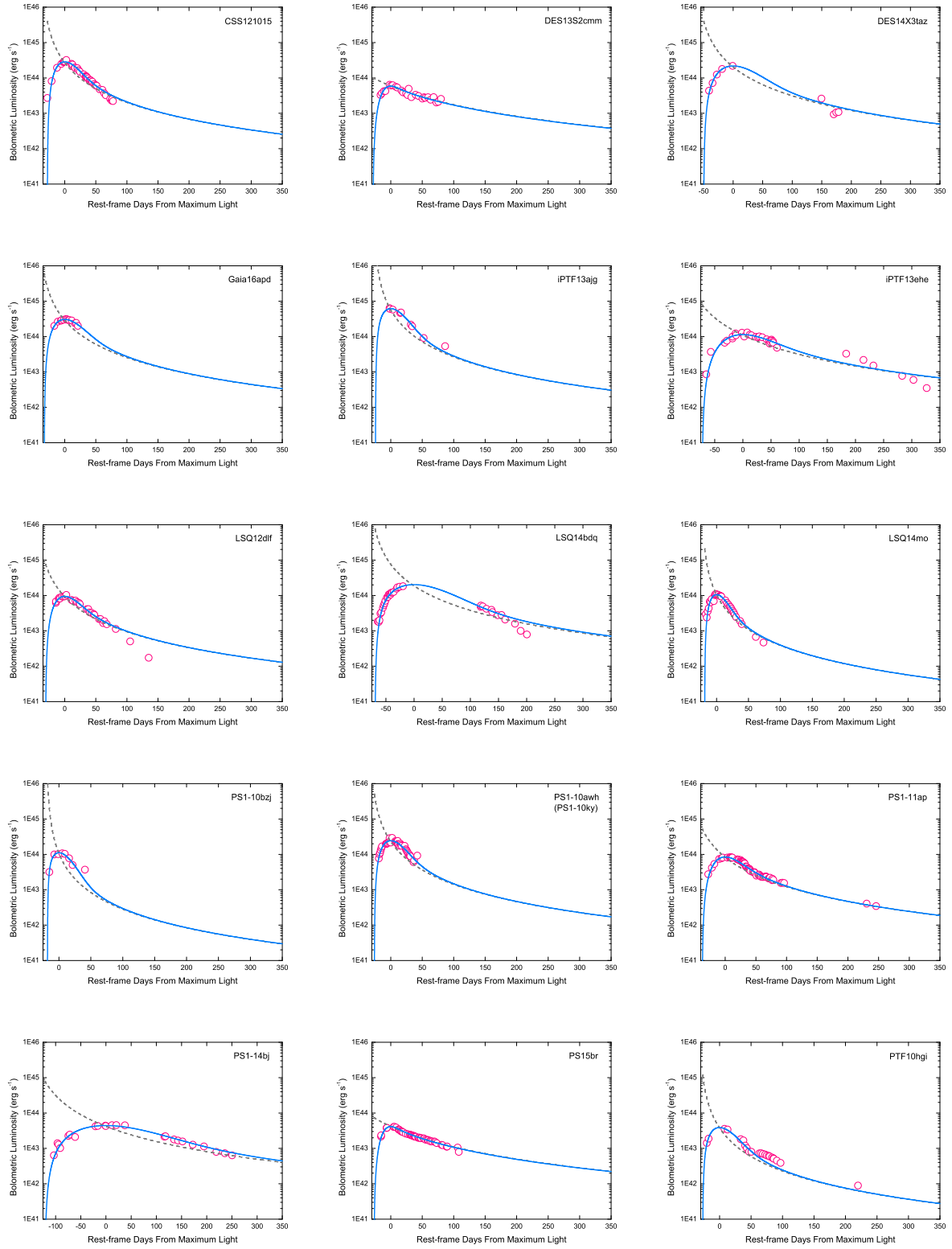


FIG. 1.— Fittings to SLSN light curves in the magnetar engine model (solid line), where individual characteristics in late observations are not taken into account. The dashed line represents the spin-down luminosity of the magnetar.

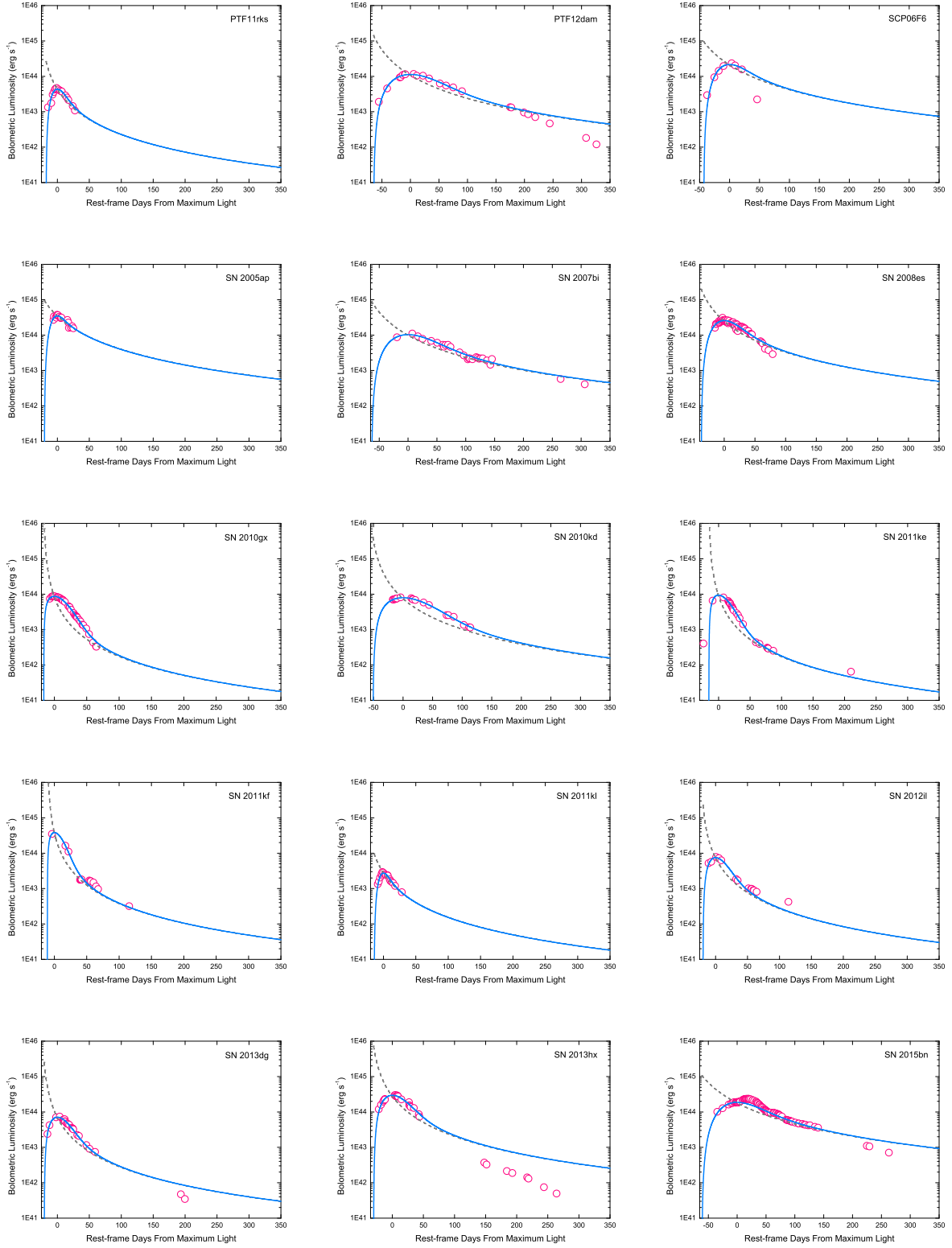


Fig. 1—Continued

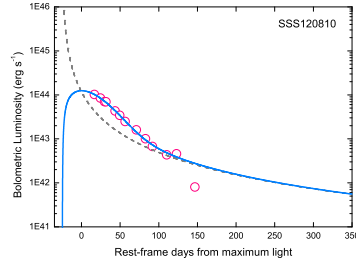


Fig. 1—Continued

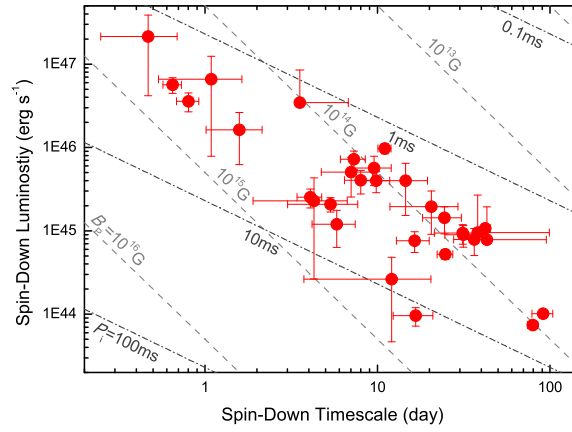


FIG. 2.— The spin-down luminosity of SLSN magnetars against the spin-down timescale. The dashed and dash-dotted lines correspond to different magnetic field strengths and initial spin periods as labeled.

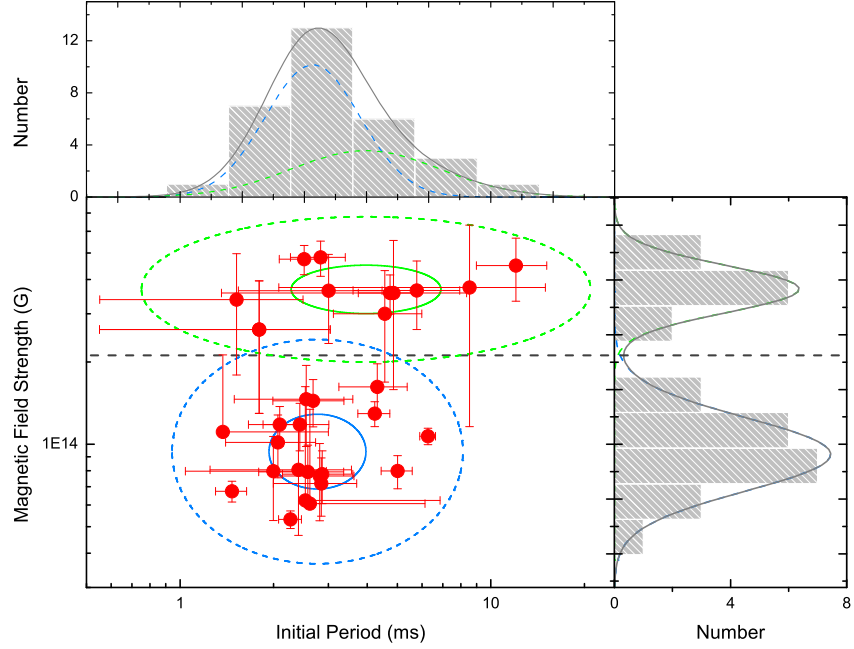


FIG. 3.— The magnetic field strengths of SLSN magnetars against the initial spin periods. The ellipses represent the  $1\sigma$  and  $3\sigma$  regions of the two subclasses defined by the log-Gaussians. The upper and right panels show that the distributions of magnetic field strengths and initial spin periods can both be fitted by the sum (solid lines) of two log-Gaussians (dashed lines). The parameters of the Gaussians are  $\mu_1 = 13.96$ ,  $\sigma_1 = 0.13$  and  $\mu_2 = 14.57$ ,  $\sigma_2 = 0.09$  for the distribution of  $\log(B_p/\text{G})$  and  $\mu_1 = 0.43$  (2.7 ms),  $\sigma_1 = 0.15$  and  $\mu_2 = 0.60$  (4.0 ms),  $\sigma_2 = 0.24$  for the distribution of  $\log(P_i/\text{ms})$ .

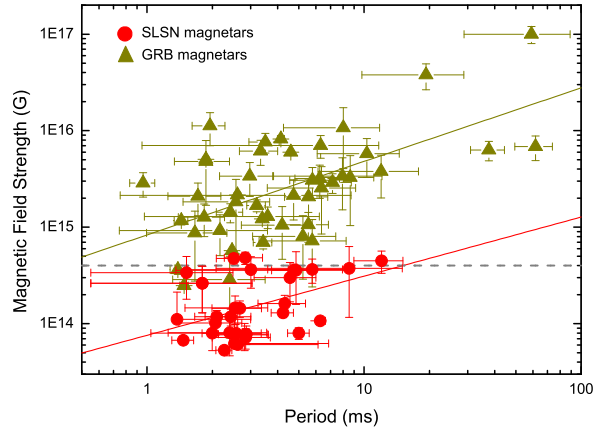


FIG. 4.— A comparison between the magnetar parameters of SLSNe and long GRBs. The two data samples can be separated by the dashed line. The solid lines represent a possible correlation between  $B_p$  and  $P_i$  of the two types of magnetars.

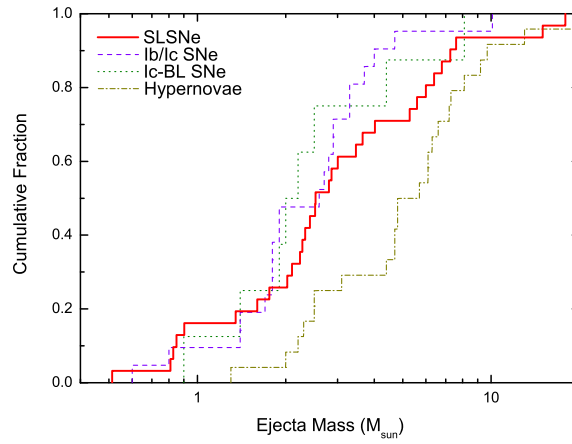


FIG. 5.— Accumulated distribution of ejecta masses of SLSNe (thick solid line). The dashed, dotted, and dash-dotted lines correspond to the cases of normal Ib/c, Ic-BL, and hypernovae, respectively.

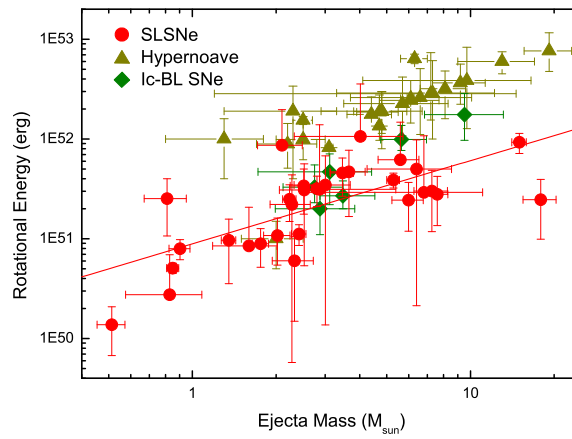


FIG. 6.— Relationship between ejected masses of SLSNe and rotational energies of SLSN magnetars. The best-fitting log-linear relation  $E_{\text{rot}} \propto M_{\text{ej}}^{0.86}$  is shown by the solid line. The masses and kinetic energies of the ejecta of Type Ic-BL supernovae and hypernovae are shown for a comparison.



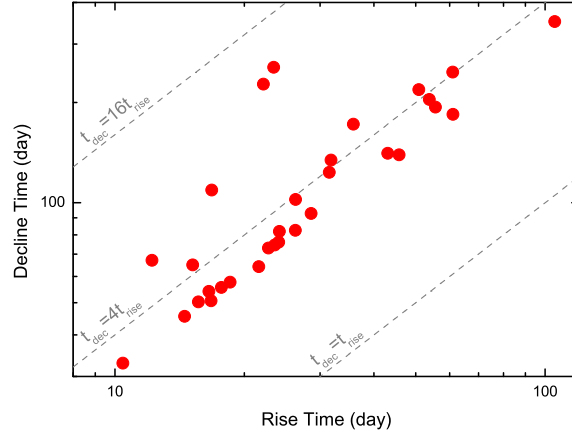


FIG. 7.— The rise timescales vs the decline timescales of SLSN light curves. **These timescales are derived from the best model fit of the light curves.** The dashed lines represent different relationships between these two timescales as labeled.

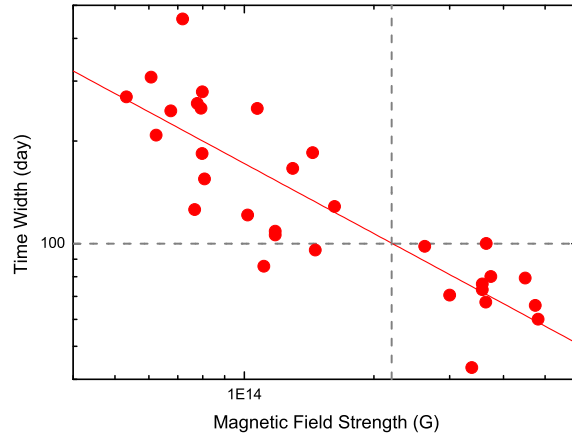


FIG. 8.— The peak widths of SLSN light curves vs the magnetic field strengths of SLSN magnetars. A possible correlation of  $\Delta t_{10\%} \propto B_p^{-0.68}$  is represented by the solid line. The dashed lines give the separating lines for the two subclasses of SLSNe at the values of  $B_p = 2.3 \times 10^{14}$  G and  $\Delta t_{10\%} = 100$  day.

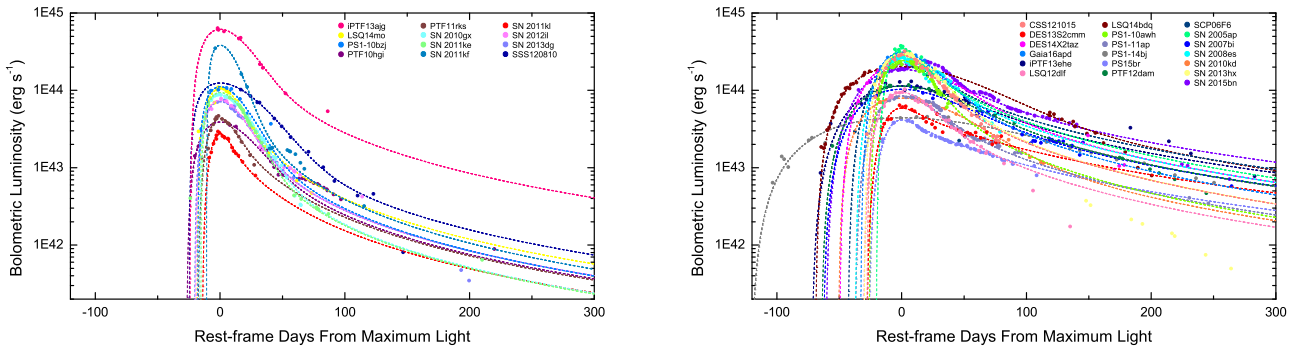


FIG. 9.— A collection of fast-evolving (left) and slow-evolving (right) SLSN light curves.

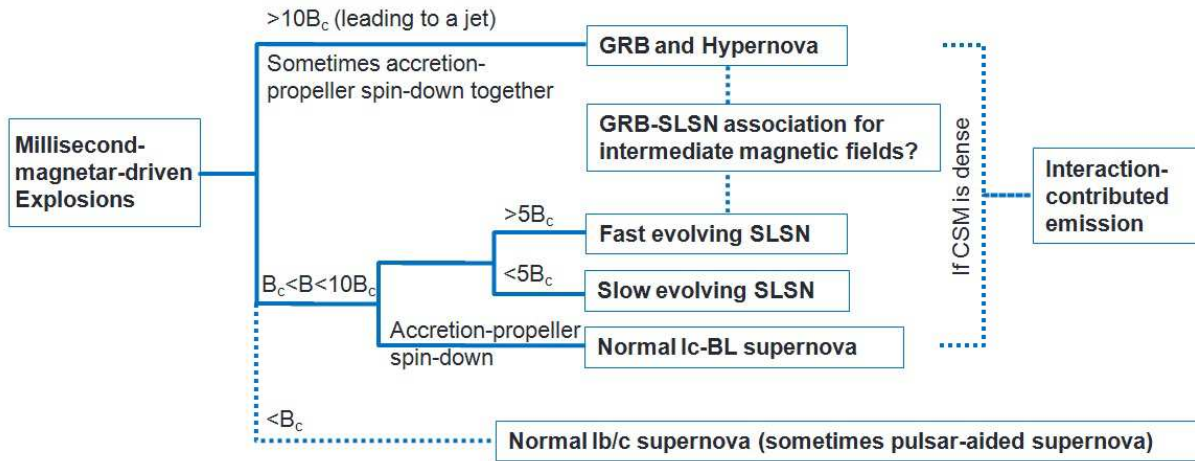


FIG. 10.— Possible connections between different magnetar-driven explosion phenomena.